*Proceedings of the 21st ICSMGE, Vienna, Austria, 14 – 19 June 2026. Pistrol, Adam & Schweiger (eds.)*
*Published by: ÖGG, Austrian Society for Geomechanics, Salzburg, Austria, ISBN 978-3-9503898-4-5*
*https://doi.org/10.53243/ICSMGE2026-877*

# Impact assessment of the seismic response of a concrete-face rockfill dam induced by the surrounding valley

**Christos Dimopoulos**, Emilios M. Comodromos, Panos Dakoulas
*Department of Civil Engineering, University of Thessaly, Volos, Greece, chrdimopoulos@uth.gr*

ABSTRACT: Dynamic numerical analyses for investigating the response of CFRD under seismic action have been performed at early 90's. Due to the available computational capacities at that period, dynamic analyses have been limited to plain strain analysis. Recent development of computational resources allowed for 3D refined mesh implementation with appropriate simulation of the most relevant mechanisms governing the interaction between the slabs and the rockfill, including slab contact activation-de-activation at vertical joints. With the intension to quantify the effect of the surrounding valley, comparative dynamic analyses were carried on a CFRD. At first a refined mesh of the computational domain was derived, including the dam and the valley with the geometrical variations at the left and right side of the dam-canyon interface, while the second series of numerical analyses a perfect rigid-plastic behavior was attributed to the valley. The response of the dam under the characteristic input motions was assessed and the behavior of the concrete face was also evaluated by establishing the range of deformations, strains, stresses and movements of the individual concrete panels and the shear strains developed in the body of the dam, revealing the impact of the surrounding valley on the seismic response.

KEYWORDS: Concrete-face rockfill dams, dam seismic response, 3D numerical simulation, concrete slab behavior.

## 1 INTRODUCTION

Dynamic numerical analyses of Concrete-Faced Rockfill Dams (CFRDs) have attracted significant research attention over the past two decades. The absence of excess pore water pressure build-up during seismic loading (Sherard & Cooke, 1987) has historically justified the emphasis of CFRD design on static performance criteria (Uddin & Gazetas, 1995). However, the 156-m high Zipingpu CFRD in China, which was subjected to the strong shallow ($M$=8) Wenchuan earthquake in May 2008, challenged the prevailing assumptions regarding the seismic behavior of such dams. The event caused extensive damage to the concrete face slabs, clearly identifying them as the most vulnerable structural component. Despite the fact that the recorded peak ground acceleration exceeded twice the design value (0.26g), the overall performance remained satisfactory. Field inspections revealed significant dislocations at the vertical joints, partial separation of the slabs from the cushion layer and concrete squeezing damage, mainly attributed to the slab's in-plane lateral movements and deformations induced by the rockfill. A comprehensive record of the observed damage patterns and corresponding instrumentation data is provided by Chen & Han (2009).

Since then, substantial research effort has been devoted to modeling the seismic behavior of CFRDs, particularly given that a considerable number of them are located in seismic regions. Advanced numerical investigations have been carried out under both 2D (Xu et al. 2015; Zou et al. 2017; Qu et al. 2019) and 3D (Kong et al. 2012; Dakoulas, 2012a; 2012b; Cen et al. 2016; Zhang et al. 2017) conditions, focusing primarily on assessing the response of the concrete face, as it is the key element ensuring the watertightness of the dam. These studies utilize damage-plasticity constitutive models to capture the effects of strain softening and accumulated damage. Furthermore, they account for the most relevant mechanisms governing the slab-rockfill interactions, including slab contact activation-de-activation at vertical joints and novel interface elements between the slabs and the cushion layer. Despite general agreement that the interaction between the embankment and the abutments influences the mode and the magnitude of the developed seismic stresses on the concrete slabs, especially under longitudinal excitations (Zhang et al. 2015), the computational domains of the above-mentioned 3D numerical studies were limited to the concrete slab's layout and the embankment body. This limitation is likely attributed to the high computational cost, as a uniform extension of the finely meshed slab zones would render such non-linear 3D analyses impractical. More recent investigations (Gong et al. 2021; Qu et al. 2021) have attempted to address this by extending the domain to include the surrounding valley using simplified V-shaped geometry. These approaches though deemed more efficient than purely embankment-based models, they still overlook the effects induced by geometrical variations along the dam–canyon interface. To overcome the challenges induced by complex terrain geometries Chen et al. (2018a; 2018b) proposed an octree-based polyhedron discretization method providing the ability for efficient mesh generation for complicated geotechnical configurations. This mesh was subsequently used to perform a 3D seismic analysis of a CFRD, providing a more realistic representation of the dam-foundation interaction. In a more recent study, Comodromos et al. (2024) conducted a detailed assessment of the seismic response of a CFRD, considering its precise 3D geometry, the surrounding valley and the reservoir by employing a gradual mesh size technique, to derive an efficient computational domain.

In this study, aiming to investigate the impact of the surrounding valley on the seismic response, a comparative 3D numerical analysis is carried out. The 150 m-high Messochora CFRD located in a narrow canyon in Greece is selected as the case study. The derived numerical model accounts for the geometrical variations along the dam-canyon interface, since the irregularity of the abutments has been shown to influence the dynamic response. Furthermore, the 1 cm-wide vertical construction joints are explicitly modeled, as they play a key role in the interaction between the adjacent slabs. Two scenarios are examined: in the first case, the computational domain includes the surrounding valley, while in the second case, the commonly adopted simplified approach of disregarding the valley is considered. Both numerical models are subjected to the same Safety Evaluation Earthquake (SSE) type characteristic input motion and the impact of the surrounding valley on the dynamic response is quantified by establishing the range of the resulting stresses, strains and deformation patterns in the individual concrete slabs and the rockfill.

## 2 DAM DESCRIPTION

### 2.1 *Geometry*

The Messochora CFRD is located in the north-central region of Greece and was designed to support a 160 MW hydropower

project, resulting in the formation of a reservoir with a total storage capacity of approximately 228 $10^6$ $m^3$. Although the construction was completed in 1995, reservoir impoundment was postponed due to revised environmental legislation and its operational use was approved only recently by the Council of State. The dam is a typical CFRD, designed in accordance with the standards of its construction period. It is the highest CFRD in Greece, with a maximum height of 150 m from the foundation level (crest altitude +775.0 m) and a crest length of 330.0 m. Fig. 1 shows a cross section of the dam at its maximum height, illustrating the layout of the rockfill materials and the corresponding instrumentation, which is currently non-operational.

The upstream slope is constant at 1.4H:1.0V, whereas the downstream slope is 1.5H:1.0V over the upper 40 meters and transitioning to 1.4H:1.0V for the rest of the height. The main rockfill materials, labeled 3B and 3C, are composed of healthy and slightly weathered limestone. The upstream face consists of 23 reinforced concrete (RC) slabs, which rest on a 4 m thick transition zone composed of well-graded gravel (zones 3A and 2B). Slab thickness increases linearly from crest to base, reaching up to 0.74 m at the dam's maximum cross section. The length varies depending on the position along the face and each slab is 15.0 m wide except for the first and last slabs, which are 7.5 m. The vertical construction joints are 1 cm wide, except at the central slab, where they were enlarged to 5 cm on either side. Reinforcement bars of Φ25/15 cm are placed along the mid-plane of each slab, with additional reinforcement provided at the slab edges to withstand anticipated stress concentration.

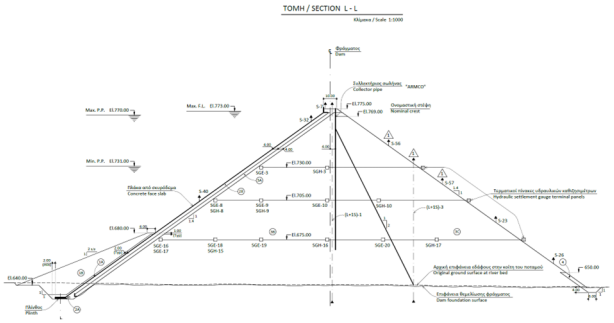


Figure 1. Cross section at the center of the Messochora dam.

## 2.2 *Constitutive models*

The plastic-hardening constitutive model (Itasca, 2023), which is widely used in geotechnical analyses was adopted to simulate the response of the rockfill during the staged construction process. Model parameters were determined through the calibration of the numerical model based on the available monitoring data at the end of the rockfill's construction. For the concrete slabs the damage-plasticity constitutive model developed by Lee & Fenves (1998) was selected. The model introduces distinct damage variables and their effect on elastic stiffness through the concept of fracture energy-based damage and modulus degradation formulation, while also accounts for stiffness recovery as a result of potential crack closure during cyclic loading. The material properties used for the concrete correspond to the typical characteristics of grade C25 concrete, with compressive strength $f_c$= 27.6 MPa, Young's modulus $E_c$= 29 GPa, tensile strength $f_t$= 3.48 MPa, density $p$= 2350 kg/$m^3$ and Poisson's ratio $v$= 0.2.

For the dynamic analyses, the hysteretic model (equivalent linear approach) was adopted for the rockfill. The shear modulus at small strains $G_0$ (for strains $\gamma < 10^{-6}$) was determined based on in-situ shear wave velocity $V_s$ measurements obtained according to the MASW method. Equations (1) and (2) define the value of $G_0$ as a function of the mean stress for the rockfill and the bedrock, respectively. During the dynamic analysis the shear modulus $G(t)$ and the damping ratio $D(t)$ were updated as a function of the range of cyclic shear strains, as Fig. 2 illustrates. Moreover, a value of 5% additional damping was assigned to the concrete slabs using the efficient Maxwell damping scheme, which provides a constant value of damping over the selected range of frequencies and overcomes the challenges posed by the implementation of the complete form of the traditional Rayleigh damping.

$$G_o = \begin{cases} 0.435 + \dfrac{3.48}{1500}\,\sigma_0' & \forall\ \sigma_0' \le 1500 \\ 3.91 & \forall\ \sigma_0' > 1500 \end{cases} \quad (1)$$

$$G_o = \begin{cases} 1.61 + \dfrac{5.67}{1560}\,\sigma_0' & \forall\ \sigma_0' \le 1560 \\ 7.28 & \forall\ \sigma_0' > 1560 \end{cases} \quad (2)$$

where $\sigma_0'$ is the effective mean stress in kPa.

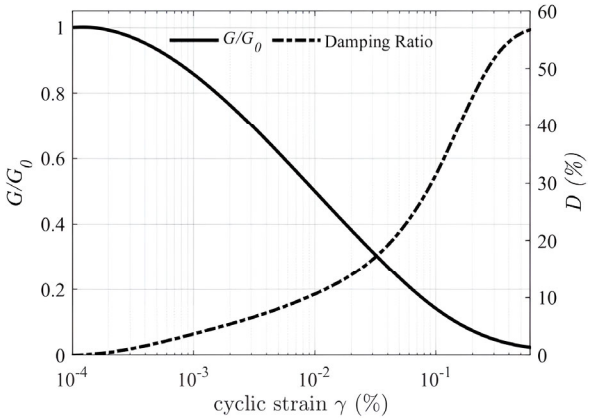


Figure 2. Modulus reduction factor and damping ratio curves for the rockfill materials as function of the cyclic shear strain in Flac3D hysteretic model.

# 3 NUMERICAL MODELING

## 3.1 *Finite model grid*

For the purposes of the comparative analysis, an advanced 3D finite mesh was prepared. The resulting mesh consists of almost 1.000.000 tetrahedral elements and captures accurately the geometrical variations along the dam-canyon interface and the concrete slabs' configuration. The interaction between the adjacent slabs depends on the contact activation-de-activation of the corresponding interface elements, thus is governed by the displacement accuracy in these regions. The 1cm-wide vertical construction joints lead to the formation of '*tiny*' elements in the vicinity of the joints. To maintain computational efficiency, a gradual size technique was employed, allowing for larger elements in regions of lower interest while preserving high resolution around these critical areas. The maximum element size was selected to ensure accurate wave propagation within the zones of the model. The resulting mesh extends up to almost one kilometer while still enabling the detailed local refinement required for the dam body. The discretization was performed utilizing the advanced meshing software *gmsh* (Geuzaine & Remacle, 2009). Fig. 3 and Fig. 4 illustrate the meshes utilized in the comparative analysis.

## 3.2 *Initial stress conditions*

A reliable dynamic analysis relies on the establishment of the initial stress conditions that reflect the current in-situ stress state. Initially the rockfill gradual construction was modelled in

75 sequential stages, each corresponding to a 2 m high increment, followed by the placement of the concrete slabs. In addition, the creep behavior of the rockfill and its effects were assessed through the evaluation of the settlement evolution curves over time. Quantifying the effects of creep is critical for capturing the stress state in the concrete slabs induced by post-construction settlements. Creep was incorporated into the analysis using a pseudotime algorithm, which considers 95% of the total density for the dam elements from the time of activation, followed by a progressive increase in a time depth of 4 years. The final stages of the multistage analysis correspond to the loading of the upstream berm and the progressive impoundment of the dam, modeled through the application of equivalent hydrostatic loads. The staged-construction simulation was performed for both cases. It should be mentioned that on static conditions disregarding the valley has a negligible influence on the predicted construction settlements due to the high stiffness of the canyon rock. Nevertheless, at the end of the impoundment phase, results indicate slightly greater displacements at the dam crest and at mid-height when the valley is included.

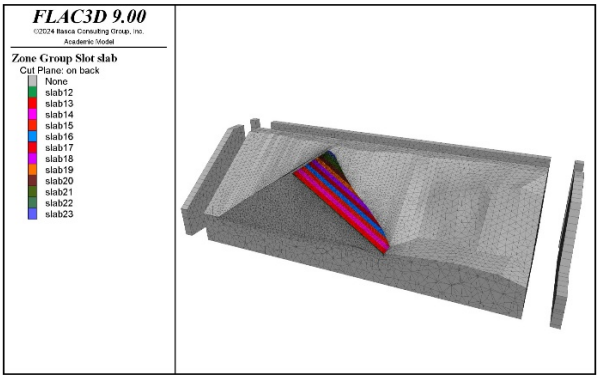


Figure 3. 3D finite model grid of the rockfill, surrounding valley and concrete slabs, consisting of approximately 1.000.000 tetrahedral elements and 36.000 interface elements.

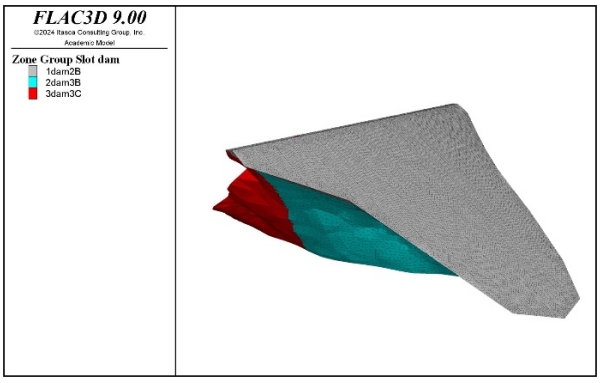


Figure 4. 3D finite model grid of the dam.

## 4 DYNAMIC SIMULATION

### 4.1 *Characteristic input motion and modeling considerations*

The Lixouri earthquake excitation was selected for the input motion, as it was deemed consistent with the site-specific characteristics. The peak ground acceleration (PGA) in the transverse direction (upstream-downstream) was scaled up to 0.48g in accordance with the Safety Evaluation Earthquake (SEE) conditions corresponding to the site's seismic zone and the importance of the structure. Accordingly, the longitudinal (parallel to the crest) and vertical components were scaled to 0.24g. Fig. 5 presents the transverse record components, after scaling and baseline correction processes. Owing to the high computational demand, associated with the small dynamic timestep, which arises from the size of the refined zones around the vertical construction joints and the implemented interface elements in these regions, only the portion of the record contributes to 5-95% of the total input seismic energy, as defined by the Arias intensity measure was used. As shown in Fig. 5, this corresponds to the interval between 2.0 and 8.0 sec. Excitation was applied as a shear and normal stress history in each direction, computed from the respective velocity components. In the simulation that included the valley, quiet boundaries were applied to the lateral and bottom edges of the model in combination with the '*free-field*' dynamic boundary condition. In contrast, for the simulation disregarding the valley, only quiet boundaries were applied along the left and right sides and at the base of the model.

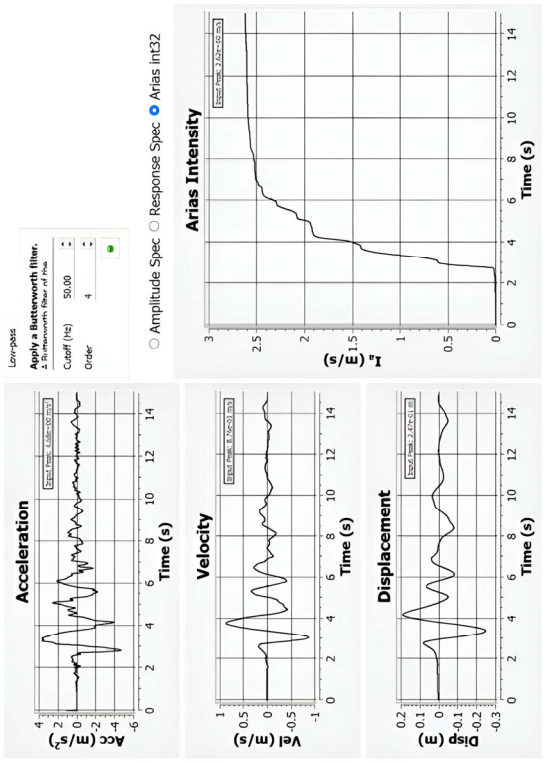


Figure 5. Transverse components of the Lixouri input motion.

### 4.2 *Hydrodynamic loading*

The effect of hydrodynamic loading on the concrete slabs was accounted for using the simplified added-mass formulation proposed by Zangar (1952). Although, modeling the reservoir with appropriate '*water*' elements (almost incompressible with zero shear modulus) provides the most accurate representation of the dam–valley–reservoir interaction, this approach is not feasible in the case of the simulation where the valley is disregarded. Therefore, only the hydrodynamic effect in the transverse direction is considered. The dynamic added mass $b$ at depth $h$ is given by Equation (3) and was integrated into the analysis through a '*user*' defined subroutine. Parameter $H$ is the reservoir depth, which in the simulations corresponds to the maximum commissioning level, $\rho_w$ denotes the water density, $A'$ is the influence area associated with each node on the upstream surface and $C_m$ is a coefficient dependent on the slope of the upstream face.

$$b = \frac{C_m}{2}\left(\left(2-\frac{h}{H}\right)+\sqrt{\frac{h}{H}\left(2-\frac{h}{H}\right)}\right)\rho_w A' H \qquad (3)$$

$$C_m = 0.735(1 - \theta°/90°) \quad (4)$$

## 5 RESULTS-EVALUATION

### 5.1 *Impact assessment of the surrounding valley*

The results of the comparative dynamic analysis are presented and evaluated in this section. The first analysis corresponds to the case where the model includes the valley (referred to as case A), while the second case (case B) represents the model where this feature is omitted. In case A the input ground motion is applied to the bottom boundary of the numerical model (Fig. 3). On the other hand, in case B a perfectly rigid domain is assumed, where the same input motion is applied simultaneously to all nodes along the left-right sides and the base of the dam. The first notable difference between the two cases lies in the dynamic characteristics of each system. In case A, the fundamental period $T_f$ is 0.41 sec, while in case B it decreases due to the fixed boundaries to 0.30 sec. Fig. 6 presents the comparison of the acceleration in the stream direction for both cases at the base of the dam, confirming that the input motion remains consistent between the two cases, which is an essential requirement for a valid comparison. Fig. 7 compares the mid-crest acceleration response in the stream direction, where the peak is slightly higher in case A and reaches the value of 1.15g.

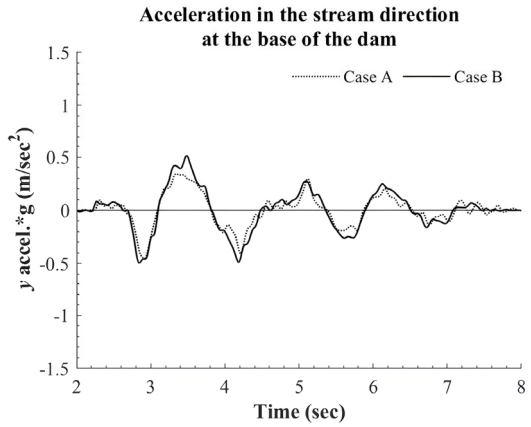


Figure 6. Acceleration response in the stream direction for the Lixouri excitation, at the base of the dam for cases A and B.

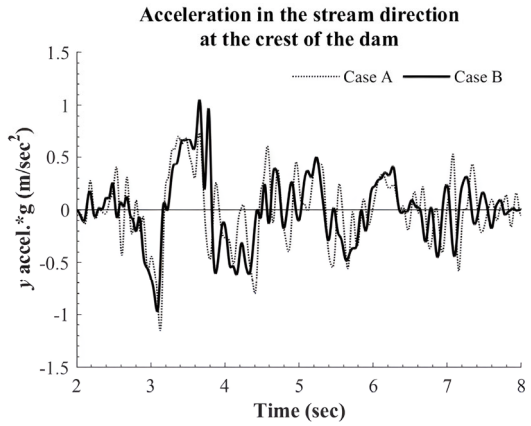


Figure 7. Acceleration response in the stream direction for the Lixouri excitation, at the crest of the dam for cases A and B.

The time history of the relative (top to bottom) horizontal displacements in the stream direction is presented in Fig. 8 for the mid-crest area. It is clear that the range of the horizontal displacements is greater in case B and at the end of the seismic action a remaining displacement of 0.19 m can be observed compared to 0.12 m in case A. Fig. 9 illustrates the time history of the shear stresses at the mid-height of the dam. The maximum value is observed in case A, while in both cases the shear stresses return close to their initial values at the end of the analysis.

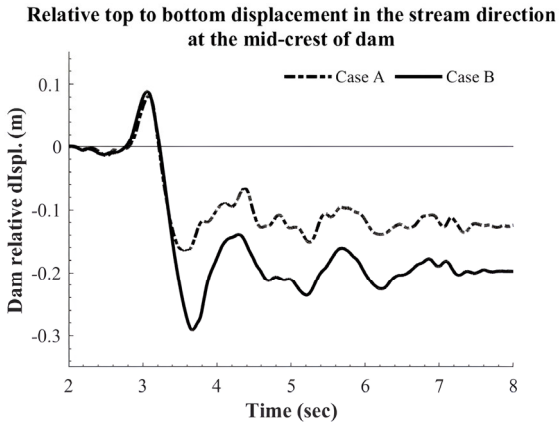


Figure 8. Relative displacement history in the stream direction at the mid-crest for cases A and B.

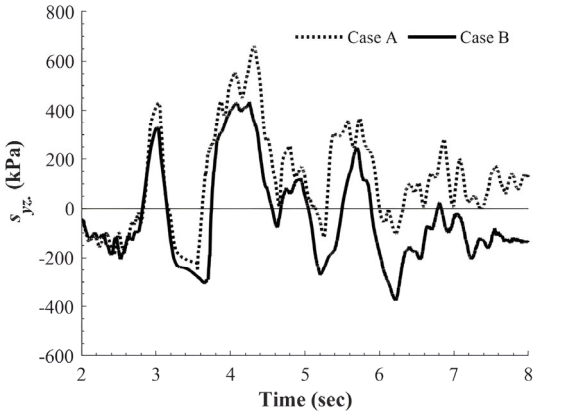


Figure 9. Shear stress history at the dam mid-height for cases A and B.

The in-plane displacement time histories for the central-right concrete slab, recorded at both the base and the top, are presented in Fig. 10. The range of the developed displacements observed in case B is noticeably greater. At the base of the slab, remaining displacements reach 7 cm in case A and 11 cm in case B, while at the top they reach 1.8 cm and 6.5 cm, respectively, indicating a slightly more rotational mode in case A for the specific concrete slab. These differences in displacements amplitude are primarily attributed to the increased energy dissipation through the hysteretic behavior of the canyon rock, along with the more efficient absorption of the outgoing waves at the model boundaries in case A.

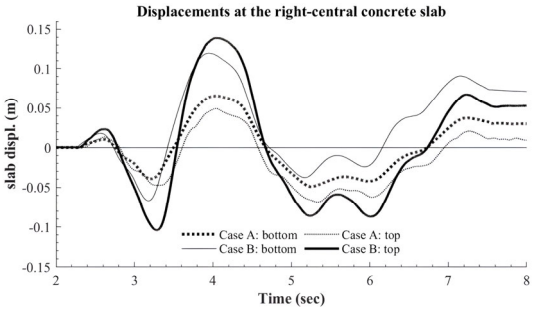


Figure 10. Displacement histories at the bottom and the top of the right-central concrete slab for cases A and B.

A comparative overview of the individual concrete slabs' displacement field and stress state at $t$= 7 sec for both case A and case B is provided in Fig. 11 and Fig. 12, respectively. By examining the contours plots in Fig. 11(a) and Fig. 12(a) it can be realized that the magnitude and the range of the slabs' in-plane displacements are higher in case B. Moreover, concrete failure is revealed in both cases. The locations of the failure are generally comparable, but the extent is significantly larger in case B. Compressive axial stresses $s_{xx}$ cover a broader region in case A, mainly concentrated at the lower part of the central slabs. Conversely, in case B, a larger portion of the slabs is subjected to tensile stresses, particularly at the crest, the base and the edges, as indicated by both the $s_{xx}$ contours in Fig. 12(b) and the maximum principal stresses $s_1$ contours in Fig. 12(c). Tensile stresses in case A become more prominent in the upper part of the slabs because of the hydrodynamic action. The shape of minimum principal stresses $s_3$ is quite similar in both cases with a slightly higher value observed in case B. These qualitative differences are mainly attributed to the effect of the canyon rock on the displacement field, which in turn governs the slabs' stress state, as the slabs due to their limited size are under the deformations imposed by the rockfill.

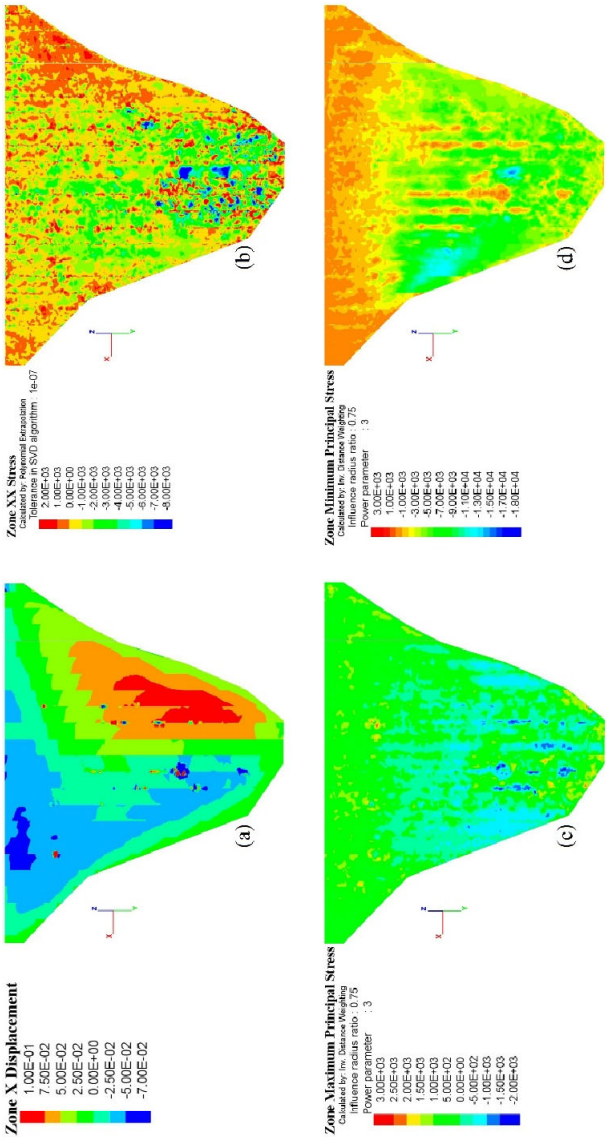


Figure 11. Case A: (a) Displacement $u_x$ (b) axial stress $s_{xx}$ (c) max. principal stress $s_1$ (d) min. principal stress $s_3$ at time $t$= 7 sec.

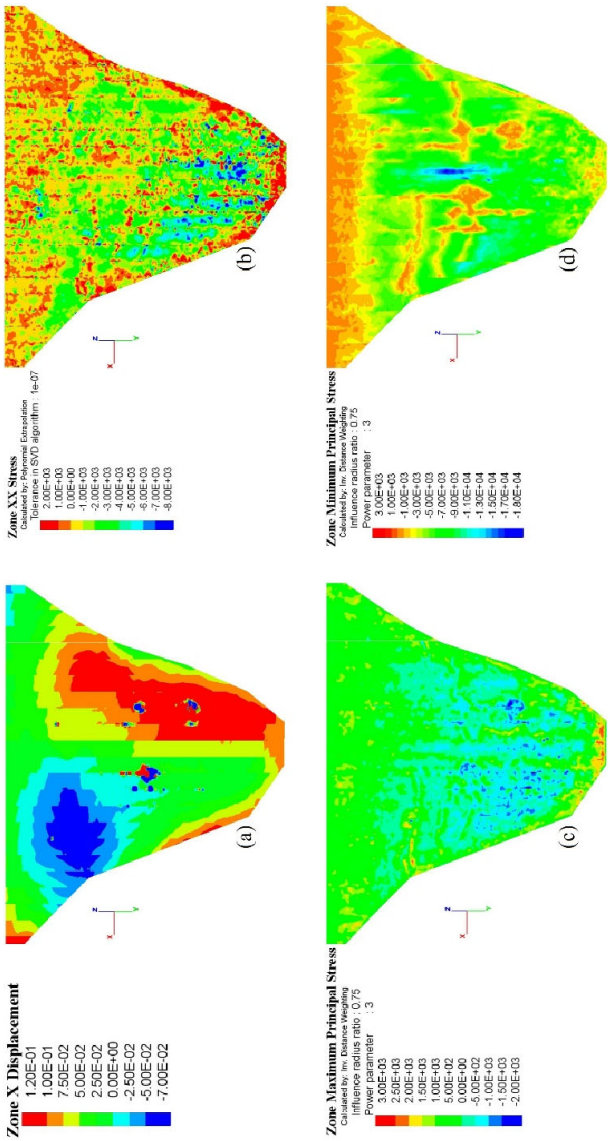


Figure 12. Case B: (a) Displacement $u_x$ (b) axial stress $s_{xx}$ (c) max. principal stress $s_1$ (d) min. principal stress $s_3$ at time $t$= 7 sec.

## 6 CONCLUSIONS

A comparative dynamic analysis using the 3D finite difference code *FLAC3D* was performed, to assess the effects of the surrounding valley on the seismic response of a CFRD, as opposed to the commonly adopted simplified approach of disregarding this feature. At first, the staged construction was simulated in detail for both configurations, to obtain reliable initial stress conditions required for the subsequent dynamic analyses. The first key observation is the modification of the system's dynamic characteristics when the valley is omitted, arising from the fixed boundary conditions applied in that case. Furthermore, it was found that disregarding the valley tends to have an unfavorable effect on the overall seismic response, as the developed displacements are higher for both the slabs and the dam body. This increase in magnitude results in noticeable variations in the stress patterns on the concrete slabs as illustrated in the stress contours at the examined timestep. The differences in the seismic response between the two cases are primarily attributed to the greater energy dissipation through the hysteretic behavior of the canyon rock, as well as to the more efficient wave radiation along the model boundaries in the full '*valley*' case. In contrast, when the valley is excluded, the

continuity of the physical domain cannot be adequately modeled. Because of this limitation there is a distortion of the outgoing propagative waves and a partial reflection back into the model. In the '*valley*' case an infinite extension of the domain is assumed at the lateral boundaries, representing more realistically the actual site conditions.

Even though the above findings highlight the influence of the surrounding valley on the seismic response, it should be mentioned that they are closely related to the specific case study characteristics. It would be unwise to generalize them without any further investigation into factors such as the frequency content, the duration and the intensity of the input motion, the geometry of the dam and the mechanical properties of both the rockfill and the canyon rock.

## 7 ACKNOWLEDGEMENTS

The research is conducted in the operating framework of the University of Thessaly Innovation, Technology Transfer Unit and Entrepreneurship Center "One Planet Thessaly", under the "Scholarship Grants to University of Thessaly Doctoral Candidates" and was funded by the Special Account of Research Grants of the University of Thessaly.

## 8 REFERENCES

Cen, W.-J., Wen, L., Zhang, Z., and Xiong, K. 2016. Numerical simulation of seismic damage and cracking of concrete slabs of high concrete face rockfill dams. *Water Science and Engineering* 9(3), 205–211.

Chen, K., Zou, D., Kong, X., and Yu, X. 2018a. An efficient nonlinear octree SBFEM and its application to complicated geotechnical structures. *Computers and Geotechnics* 96, 226–245.

Chen, K., Zou, D., Kong, X., and Zhou, Y. 2018b. Global concurrent cross-scale nonlinear analysis approach of complex CFRD systems considering dynamic impervious panel–rockfill material–foundation interactions. *Soil Dynamics and Earthquake Engineering* 114, 51–68.

Chen, S., and Han, H. 2009. Impact of the '5.12' Wenchuan earthquake on Zipingpu concrete face rock-fill dam and its analysis. *Geomechanics and Geoengineering* 4(4), 299–306.

Comodromos, E.M., Dakoulas, P., Dimopoulos, C., Russo, G., Dimou, C.K., and Papachatzaki, C. 2024. Seismic response evaluation of a CFRD considering its precise 3D geometry and the surrounding valley. *Proc. International Symposium on Dams and Earthquakes*, 7th Meeting of the EWG, Athens, 318-329.

Dakoulas, P. 2012a. Nonlinear seismic response of tall concrete-faced rockfill dams in narrow canyons. *Soil Dynamics and Earthquake Engineering* 34(1), 11–24.

Dakoulas, P. 2012b. Longitudinal vibrations of tall concrete-faced rockfill dams in narrow canyons. *Soil Dynamics and Earthquake Engineering* 41, 44–58.

Geuzaine, C., and Remacle, J.-F. 2009. Gmsh: A three-dimensional finite element mesh generator with built-in pre- and post-processing facilities. *International Journal for Numerical Methods in Engineering* 79(11), 1309–1331.

Gong, J., Zou, D., Kong, X., Liu, J., and Chen, K. 2021. The simulation of high compressive stress and extrusion phenomenon for concrete face slabs in CFRDs under strong seismic loads. *Soil Dynamics and Earthquake Engineering* 147, 106792.

Itasca Consulting Group, 2023. *FLAC3D*: *Fast Lagrangian Analysis of Continua*. Version 9. Minneapolis: Itasca Consulting Group.

Kong, X., Zhou, Y., Zou, D., Xu, B., and Yu, L. 2012. Numerical analysis of dislocations of the face slabs of the Zipingpu concrete faced rockfill dam during the Wenchuan earthquake. *Earthquake Engineering and Engineering Vibration* 10, 581–589.

Lee, J., and Fenves, G. 1998. Plastic-damage model for earthquake analysis of dams. *Earthquake Engineering & Structural Dynamics* 27(9), 937–956.

Qu, Y., Zou, D., Chen, K., and Liu, J. 2021. Three-dimensional refined analysis of seismic cracking and anti-seismic measures performance of concrete face slab in CFRDs. *Computers and Geotechnics* 139, 104376.

Qu, Y., Zou, D., Kong, X., Liu, J., Zhang, Y., and Yu, X. 2019. Seismic damage performance of the steel fiber reinforced face slab in the concrete-faced rockfill dam. *Soil Dynamics and Earthquake Engineering* 119, 320–330.

Sherard, J.L., and Cooke, J.B. 1987. Concrete-face rockfill dam: I. Assessment. *Journal of Geotechnical Engineering* 113(10), 1096–1112.

Uddin, N., and Gazetas, G. 1995. Dynamic response of concrete-faced rockfill dams to strong seismic excitation. *Journal of Geotechnical Engineering* 121(2), 185–197.

Xu, B., Zou, D., Kong, X., Hu, Z., and Zhou, Y. 2015. Dynamic damage evaluation on the slabs of the concrete faced rockfill dam with the plastic-damage model. *Computers and Geotechnics* 65, 258–265.

Zangar, C.N. 1952. *Hydrodynamic pressures on dams due to horizontal earthquake effects*. Washington, DC: Bureau of Reclamation, U.S. Department of the Interior.

Zhang, J.-M., Yang, Z., Gao, X., and Zhang, J. 2015. Geotechnical aspects and seismic damage of the 156-m-high Zipingpu concrete-faced rockfill dam following the Ms 8.0 Wenchuan earthquake. *Soil Dynamics and Earthquake Engineering* 76, 145–156.

Zhang, Y., Kong, X., Zou, D., and Xu, B. 2017. Tensile stress responses of CFRD face slabs during earthquake excitation and mitigation measures. *International Journal of Geomechanics* 17(12), 1–12.

Zou, D., Han, H., Liu, J., Yang, D., and Kong, X. 2017. Seismic failure analysis for a high concrete-face rockfill dam subjected to near-fault pulse-like ground motions. *Soil Dynamics and Earthquake Engineering* 98, 235–243.